Quaternary Research 80 (2013) 447–458

Contents lists available at ScienceDirect

Quaternary Research

journal homepage: www.elsevier.com/locate/yqres

Early Holocene monsoonal fluctuations in the Garhwal higher Himalaya as inferred from multi-proxy data from the Malari paleolake

Pradeep Srivastava [a,*], Anil Kumar [a], Akanksha Mishra [b], Narendra K. Meena [a], Jayant K. Tripathi [b], Y.P. Sundriyal [c], Rajesh Agnihotri [d], Anil K. Gupta [a]

[a] Wadia Institute of Himalayan Geology, 33 GMS Road, Dehradun 248001, India
[b] School of Environmental Sciences, Jawaharlal Nehru University, New Delhi 110067, India
[c] Department of Geology, H.N.B. Garhwal University, Srinagar 246174, India
[d] National Physical Laboratory, New Delhi 110012, India

ARTICLE INFO

Article history:
Received 3 August 2012
Available online 27 August 2013

Keywords:
Paleolake profile
Semiarid Himalaya
Organic phosphorus
Mineral susceptibility
Indian Summer Monsoon
Solar forcing

ABSTRACT

A 4.9-m-thick lake sequence, formed due to the landslide damming of a stream in the semiarid Garhwal Himalaya, was studied to understand past monsoonal variations in the region. The Optically Stimulated Luminescence (OSL) chronology indicates that the lake existed between ~12 and ~7 ka ago. Chronologically constrained trends of sand percent, organic phosphorus (OP), apatite inorganic phosphorus (AIP) and parameters of environmental magnetism were measured in the paleolake profile. Measured proxies indicate that the Indian summer monsoon ameliorated in the early Holocene after 12 ka cooling, and it appears that all the proxies from the lake have captured this globally recognized early Holocene warming. Four phases of wet conditions (intensified monsoon) are recognized at ~11.5 ka, ~11–10.5 ka, ~10–9 ka and ~8–7 ka with maximum uncertainties of ~1000 years. The wet phases are characterized by high magnetic susceptibility, increased OP and reduced AIP. In an attempt to understand the primary forcing of the sharp fluctuations in monsoonal activity in the region, we show that changes in magnetic susceptibility match variations of residual atmospheric $\delta^{14}C$, suggesting a role for solar variability as an explanation of climatic variability.

Introduction

The landscape of the Himalaya is a result of precipitation and tectonic processes occurring on a variety of time scales. During long cold and dry spells, the vegetation cover on steep slopes is depleted leading to the production of loose soil and debris. During wetter phases the loose debris and soil are mobilized down the slope, particularly as landslides that block streams, creating landslide dammed lakes. These events are often found in sedimentary archives flanking the rivers and represent phases of intense Southwest (SW) Indian Monsoon (Bookhagen et al., 2005; Sundriyal et al., 2007; Juyal et al., 2009; Phartiyal et al., 2009). The sedimentation in the Himalayan lakes is often continuous and their study thus offers an opportunity to understand the sharp climatic variations in the past. The dated profiles of these lakes help to understand not only the climatic variability through time but also the climate forcing factors and their global linkages.

Paleolakes have been studied from the Lesser Himalayas of Kumaun (Kotlia et al., 1997a) and in the upper Indus Valley (Skardu in Ladakh) to understand past climatic variations (Burgisser et al., 1982; Cronin, 1989; Fort et al., 1989; Shroder et al., 1989; Bagati et al., 1996; Kotlia et al., 1997b; Shukla et al., 2002). However, most of these studies focused largely on landscape evolution and the causes of formation of paleolakes. Studies also indicated that ^{14}C dating is not suitable for paleolake sequences located in carbonate-dominated country rocks. Recent investigations using luminescence ages in the Goting Lake sequence suggest that the lacustrine environment spanned a range of 20–11 ka (Juyal et al., 2004, 2009) instead of 40–30 ka based on ^{14}C ages, demonstrating that radiocarbon dates are overestimated due to old carbon contamination. Lately, Tso Kar lake, located in the Zanskar ranges of the arid Himalaya, was studied to decipher the latest Pleistocene–Holocene climatic conditions during the last 15 ka (Wünnemann et al., 2010). Since the Higher Himalaya is a seismically active zone that is impacted by intense rainfall during intensification of the monsoon, few lakes exist. Nonetheless there are some lakes that contain important climatic archives because of their sensitivity to minor changes in temperature and precipitation. Also, reconstructions of monsoon history from this region are important to provide better understanding of the spatial and temporal changes and forcing factors responsible for monsoon dynamics at time scales beyond the instrumental era.

The studies undertaken so far utilized sedimentology, pollen taxonomy, environmental magnetism and chemical indices involving major, trace and rare earth elements. The present study, however, focuses on (a) the variability in organic/inorganic phosphorus and (b) environmental magnetism in response to prevailing paleoclimate/monsoonal

* Corresponding author.
E-mail address: Pradeep@wihg.res.in (P. Srivastava).

0033-5894/$ – see front matter © 2013 University of Washington. Published by Elsevier Inc. All rights reserved.
http://dx.doi.org/10.1016/j.yqres.2013.07.006

conditions. We also attempt here to identify the dominant climatic force responsible for the observed changes in the proxy data.

Phosphorus is a limiting nutrient for productivity in aquatic and terrestrial ecosystems (Broecker, 1982; Tiessen et al., 1984; Filippelli, 2002; Ruttenberg, 2007). In the biogeochemical cycle of phosphorus, the weathering of apatite in rock is the major source of phosphorus for living organisms. At high altitudes, the apatite-bound inorganic phosphorus is eroded during glacial conditions and organic-bound phosphorus is supplied from the soils during humid conditions. Therefore, the nature of phosphorus species supplied from a catchment depends on cooler/dry or warmer/wet climatic conditions (Filippelli et al., 2006 and references therein). If the digenetic processes did not alter the phosphorus species (from organic-bound to iron-bound) and the lake remained oligotrophic during sedimentation, the sedimentary deposits may serve as important archives for understanding past climate (Filippelli and Souch, 1999; Filippelli et al., 2006).

The phosphorus fractions (inorganic and organic), as proxies for paleoclimate in lake sediments of glacial–periglacial regions, have been extensively exploited, for example in Canada (Slaymaker et al., 2003; Filippelli et al., 2006; Teed et al., 2009), in southern California and Illinois, USA (Filippelli and Souch, 1999; Kirby et al., 2007), and in Costa Rica. No such attempts have been made to understand the dynamics of different species of phosphorus in the Indian subcontinent. By virtue of its location in a semiarid climatic zone towards the northern limit of the SW Indian Monsoon, it is reasonable to presume that any perturbation in climate could be manifested as changes in organic productivity and/or the sediment budget. Accordingly, this study attempts to infer climatic fluctuations using three independent climate proxies namely, phosphorus speciation, mineral susceptibility and grain size from a sedimentary profile in a landslide dammed lake located in the semiarid Higher Himalaya. The sequence has been dated to ~12 to ~7 ka using the Optically Stimulated Luminescence (OSL) technique. The results are compared with the proxy records of the SW Indian monsoon from other well-dated continental and marine records. In addition, an attempt is made to understand the primary forcing factors driving precipitation changes in the area.

Study area and field setup

The lake sequence near Malari is located at an altitude of 2922 m asl (lat. 30°40′11.11″N; long. 79°52′53.69″E) towards the north of the South Tibetan Detachment System (STDS), along the Dhauliganga River. The country rock comprises sedimentary rocks of the Tethyan sequence (Figs. 1A, B), composed of bedded black shale, slate, phyllite and quartzite of Precambrian age, calcareous sandstone and limestone of Cambrian to Ordovician age, and purple limestone, shale and quartzite of Silurian age (Sinha, 1989). Data from the Tropical Rainfall Measuring Mission (TRMM) shows that towards the mountain front the annual rainfall is ~1300 mm, decreasing to ~670 mm at Malari (Fig. 1C). Therefore, the studied section lies at the northern extremity of the influence of the SW monsoon.

The valley at the study site is wide and has a fill terrace made up of basal matrix-supported angular/rounded gravels overlain by 4.9 m of fine-grained lacustrine sediments (Fig. 2). This is overlain by 12–16 m of matrix-supported angular gravels. The sequence was described at two different locations (Fig. 2).

Methods

The sedimentary facies of the lake sequence were documented by using grain size, physical structure, and the characteristics of the matrix, color, and degree of bioturbation. A total of 49 samples were collected from the lacustrine section. Estimation of (i) organic and apatite inorganic phosphorus fractions, (ii) environmental magnetic parameters, namely magnetic susceptibility (χlf), anhysteretic remnant magnetization (ARM), isothermal remnant magnetization (IRM), coercivity of remanence ($B_{(0)}$cr) and S-ratio, and (iii) grain size was studied using sieving and pipette analysis. In order to constrain the chronology of the studied sequence, six samples were dated using Optically Stimulated Luminescence.

Phosphorus estimation

For determination of the different fractions of phosphorus in the lake sediments, we followed the *Standards, Measurements and Testing* (SMT) *Protocol* (Ruban et al., 2002). This protocol is a modification of the method described by Williams et al. (1971) that was originally developed for soft sediments. The protocol involves extraction of organic phosphorus (OP), apatite inorganic phosphorus (AIP) and non-apatite inorganic phosphorus (NAIP) fractions of phosphorus. To determine the different fractions, 0.2 g of sample was used for extraction. For determination of OP, the IP was first extracted by shaking the sample for 16 h in 20 ml of 1 M HCl. The residue of the sample was calcined at 450 °C for 3 h and again extracted using 1 M HCl for 16 h at 25 °C for OP. For NAIP determination, extraction used 1 M NaOH for 16 h. An aliquot of the supernatant was treated with 3.5 M HCl to determine NAIP. The residue of this extraction was extracted for AIP using 1 M HCl for 16 h. The concentrations of the different fractions in the extractants were determined using ICP-AES (Jobin Yvon ULTIMA 2) at Jawaharlal Nehru University, New Delhi. The precision of determination of OP and AIP was better than 5%, while for NAIP it was 10–15%. The use of NAIP as a proxy is less reliable here as compared to OP and AIP. Thus we only use OP and AIP fractions for further interpretations.

Environmental magnetic parameters

To quantify changes in magnetic mineralogy, sediment samples were first packed into 10-cm^3 nonmagnetic (styrene) pots. Magnetic susceptibility (χlf) was measured at two frequencies (0.47 and 4.7 kHz) using a Bartington MS2B laboratory sensor. Isothermal remnant magnetization (IRM) was measured by inducing a forward magnetic field of 100 to 1200 mT in an impulse magnetizer at 100 mT incremental sequences. A backward magnetic field of 10 mT, 20 mT, 30 mT, 50 mT, 100 mT and 300 mT was also imposed to demagnetize the sample. The magnetic moment was measured by the Molspin Minispin magnetometer. The IRM_{1000} is referred to as Saturation isothermal remnant magnetization (SIRM). Anhysteretic remnant magnetization (ARM) was grown with a peak alternating field of 99 mT in the presence of a DC field of 0.1 mT. The coercivity of remanence ($B_{(0)}$cr) was calculated from the IRM acquisition curve. ARM is taken as a proxy for concentration of the Stable Single Domain (SSD) magnetic grains of physical size of 0.1 μm. The S-ratio is obtained by dividing the IRM-300 by the SIRM.

Optically Stimulated Luminescence (OSL) dating

Six samples (5 samples from the lake sequence and 1 from an adjacent section) were dated using OSL. Dating of the terrace sediments and the lacustrine units in particular was carried out to deduce (i) the timing of lake formation and (ii) timeframe of past climatic events. The age at the bottom marks the time when the river was blocked and that at the top of the lacustrine unit indicates when the lake was breached. Samples were collected using opaque stainless steel pipes. This technique relies on the presumption that, prior to burial, geological luminescence stored in the minerals was zeroed by day light exposure during erosion and transportation (Aitken, 1998). However, steep gradients and turbulence may result in inhomogeneous bleaching of fluvial sediments that may induce errors in age estimation. The uncertainty arising due to this is generally tackled by reducing the size of aliquots and by considering the lowest paleodoses for age estimation (Srivastava et al., 2008; Ray and Srivastava, 2010). Poor or inhomogeneous bleaching of sediments is expressed as a wide scatter in paleodose estimates (Preusser et al., 2009). In the present work, we have used the least

https://doi.org/10.1016/j.yqres.2013.07.006 Published online by Cambridge University Press

10% of the paleodoses, usually the data from 2–3 aliquots out of 30 (Fig. 3). Feldspar contamination is another major problem in these samples, as this mineral, being brighter in terms of luminescence, tends to mask the signal arising from quartz. This was checked by performing the Infrared Stimulated Luminescence (IRSL) test (as IRSL stimulates only feldspars) and any sample with more than 150 IRSL counts was subjected to an additional 10 min of HF treatment.

The quartz fraction from the samples was extracted by sequential chemical treatment following Srivastava et al. (2008). The fraction was sieved to separate the 90–150 μm size range and etched using 40% HF for 80 min, followed by 12 N HCl treatment for 40 min to remove the alpha irradiated surface layers. IRSL measurement was performed on every sample to check for feldspar contamination. Samples showing IRSL counts of more than 100 were subjected to an additional step of density separation and HF etching for 20 min. The grains were mounted on stainless-steel disks using Silko-Spray silicone oil. Luminescence measurements were made on a Riso TL/OSL-12 system with an array of blue LEDs as a source for stimulation. Schott BG-39 and Hoya U-340 optical filters in front of an EMI 9235 QA photomultiplier tube were used for photon detection.

OSL was recorded for 40 s at 125 °C. A $^{90}Sr/^{90}Y$ beta source delivering a dose rate of 6.7 Gy min^{-1} was used for irradiation. A 5-point single aliquot regeneration (SAR) protocol, suggested by Murray and Wintle (2000), was used to determine the paleodose. An additional step of IRSL cleaning (for 100 s at 60 °C) was introduced before every OSL measurement. This was done to reduce any signal coming from feldspar (Jain and Singhvi, 2001). A preheat of 220 °C per 10 s and a cut heat of 160 °C for test doses were used. Thirty disks were used for measurement. Out of which the weighted mean of the lowest 10% paleodose values was used for age calculations (Galbraith et al., 1999; Srivastava et al., 2009). The paleodose estimate is based on aliquots with a recycling ratio of 1.1–0.9. The initial 2 channels (1 channel = 0.16 s of OSL measurement) of the shine down curve were used for analysis. Uranium, thorium and potassium concentrations were determined by XRF analysis and radioactive equilibrium was assumed. For the cosmic ray exposure at an elevation of ~3000 m, the dose rate on the surface at this latitude has been computed to be ~350 μG yr^{-1}, reducing to 30 μG yr^{-1} at a depth of 20 m. Given an exponential decrease of the dose rate, a constant value of 190 ± 30 μG yr^{-1} has been assumed for dose rate calculations in this study (Beukema et al., 2011).

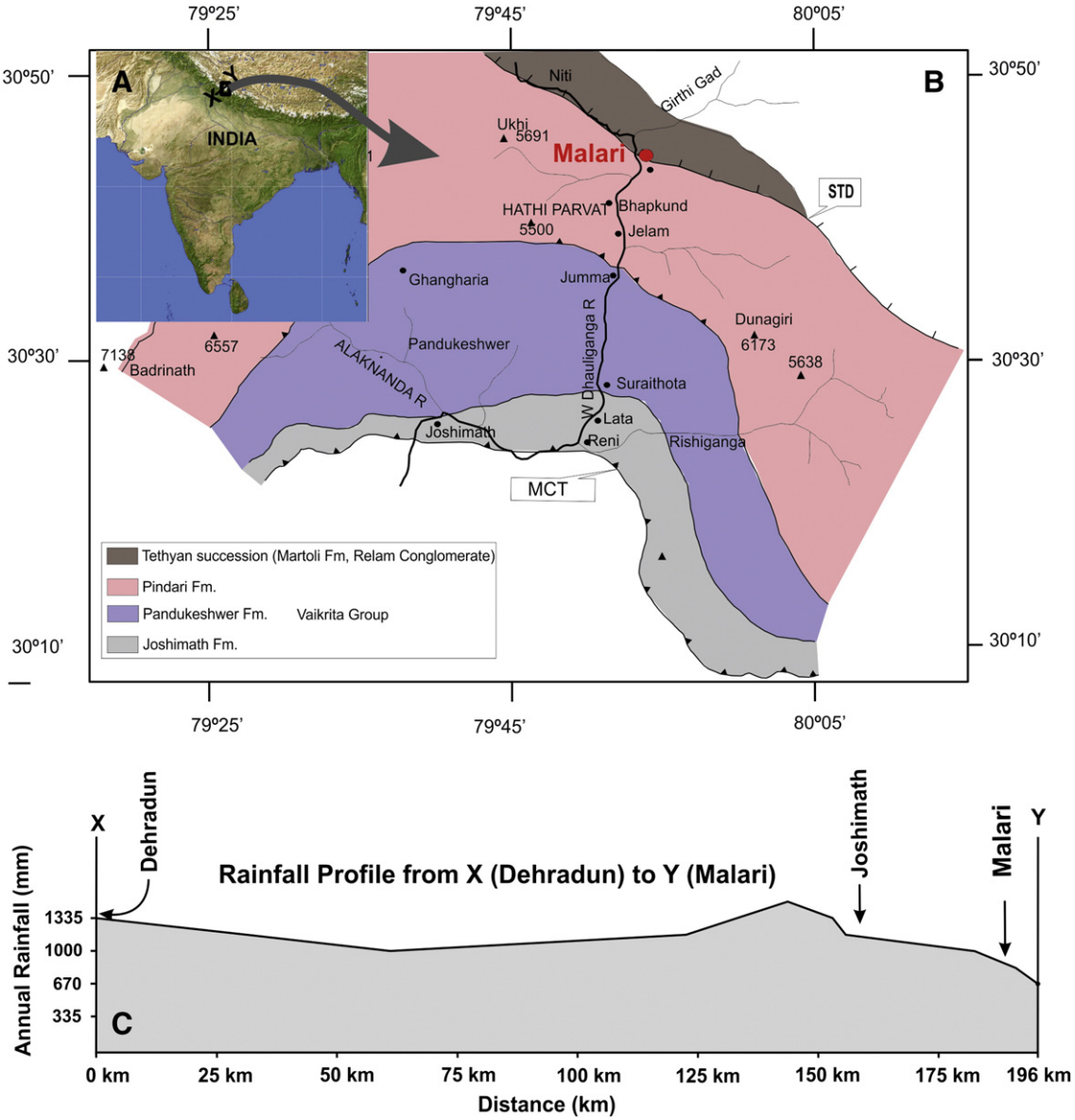

Figure 1. (A) Location of the study area. X-Y is a section line referred to in Figure 1C. (B) Location and geological map of the study site. (C) Rainfall variation along the X-Y transect indicating semiarid conditions at Malari. This suggests that the Malari Lake lies at the northern extremity of the SW Indian Monsoon.

https://doi.org/10.1016/j.yqres.2013.07.006 Published online by Cambridge University Press

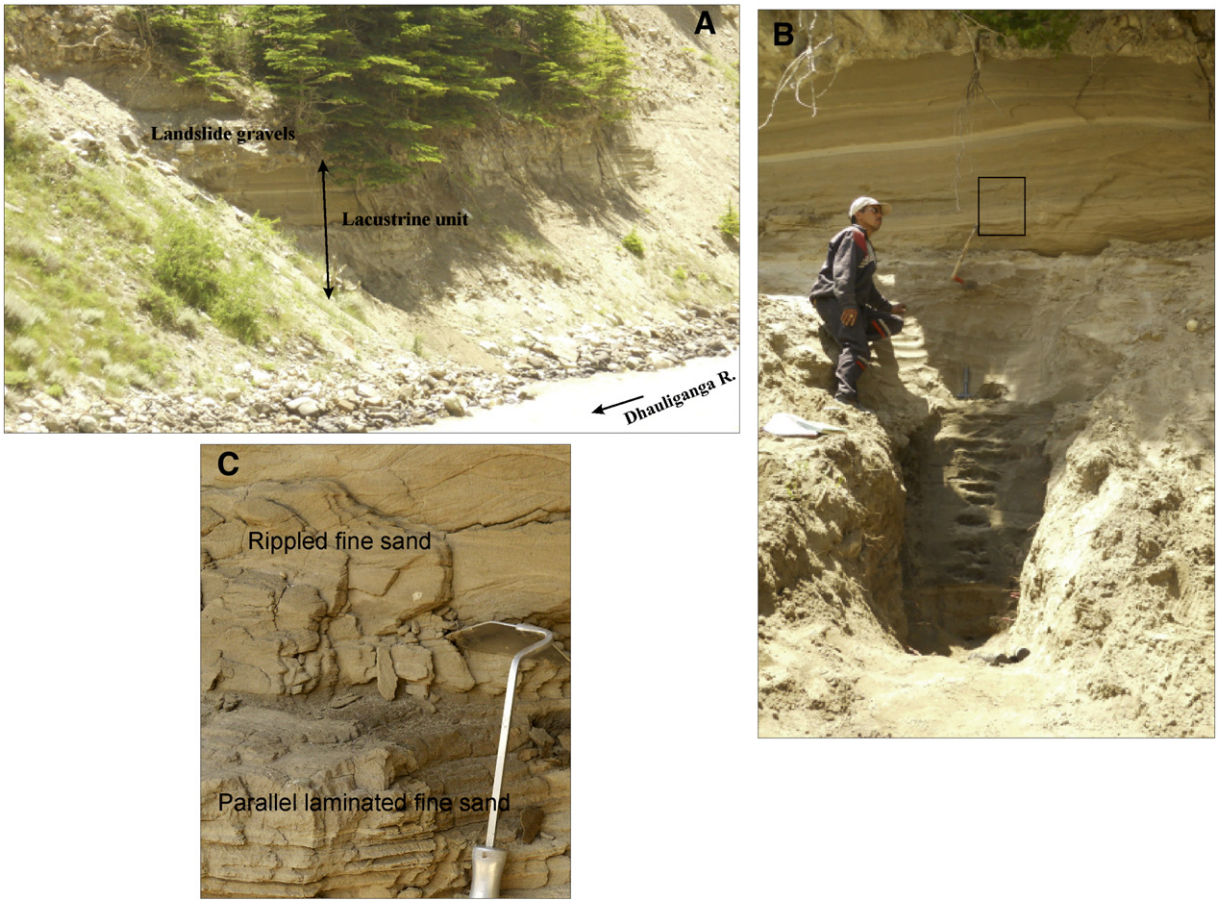

Figure 2. Photograph showing (A) general lithostratigraphy of section one. (B) Closer view of the lacustrine unit. Inset refers to Figure 2C. (C) Closer view of the fine-grained lacustrine lithologies.

Results

Lake sequence

The Dhauliganga (DG) valley near its confluence with Girthi Gad has one fill terrace composed of ~25 m with three lithofacies i.e. (i) matrix-supported angular gravels, (ii) well-rounded imbricated gravels, and (iii) silty fine sand.

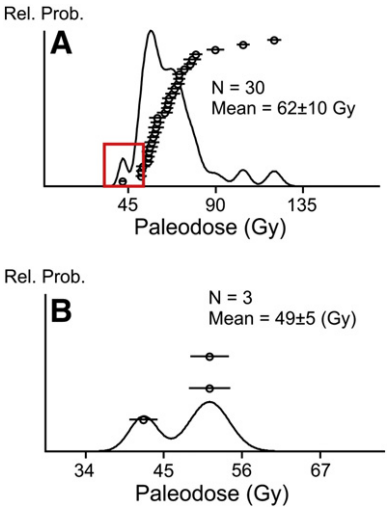

Figure 3. Probability distribution of paleodose data for sample LD-807. (A) Wide distribution of paleodoses indicating heterogeneous bleaching of geological luminescence. (B) Least 3 paleodoses (inset), which represent the most bleached population of grains, and are used in the final age estimation.

Matrix-supported angular gravel units, 2–18 m thick, are composed of ~25% matrix and angular clasts sourced from locally exposed rocks. The clasts are poorly sorted, ranging from a few centimeters to at times more than a meter in size. Laterally, these units are extensive and form erosional lower and upper contacts, where no bedding structures are visible. This lithofacies is interpreted as a product of debris flow during landslides (Ray and Srivastava, 2010).

Well-rounded imbricated gravel units, 1–8 m thick, are composed of moderately well sorted, well-rounded, imbricated gravels. The matrix is as low as 10%. This is a product of channel alluviation through aggradation on a bar.

Silty fine sand units are 4–5 m thick, composed of very fine sand with varying percentages of silt and clay vertically. Internally these units show ripple cross laminations, parallel laminations and sand/silty clay couplets (Figs. 2B, C). This is interpreted as aggradation in a lacustrine environment subsequent to the landslide damming of a channel.

Section one (30º40′11.11″ N; 79º52′53.69″E), located on the right bank of the Dhauliganga, has an ~2-m-thick unit of matrix supported angular gravels from the base upwards followed by 4.9 m of silty fine sand (Figs. 2A,B). This is overlain by 7.9 m of well-rounded imbricated gravels that in turn is overlain by 12 m of matrix-supported angular gravels (Fig. 4A). Figure 4B shows the detailed stratigraphy of the lacustrine unit, which is composed of fine-grained rippled and parallel laminated sand that often alternates with parallel-bedded units of clayey silt and fine sand.

Section two (30º42′17.21″N; 79º52′56.14″ E) located on the right bank of Girthi Gad, is ~26 m thick that starts with a unit of fluvial gravels

https://doi.org/10.1016/j.yqres.2013.07.006 Published online by Cambridge University Press

followed by a lacustrine unit capped by ~16 m of landslide debris (Fig. 4C).

Luminescence ages and the chronological framework

The chronological framework (age–depth model; Fig. 5) was set up by interpolating five OSL ages, where the oldest age of the lacustrine unit is ~12 ka while the uppermost and youngest unit is dated to ~7 ka. All five dates are in stratigraphic order (Table 1). The sample collected from section two (LD-829) yielded an age of ~9 ± 2 ka, which is in conformity with that of section one. We analyzed three samples for ^{14}C dating using both bulk and organic matters, using the Radiocarbon facility of the Physical Research Laboratory, India. All the ages were much older than those from OSL (Fig. 4B). The results of ^{14}C dating are given in Table 2. The ^{14}C ages of 33, 29 and 44 ^{14}C ka BP from bottom upwards are not in stratigraphic order and are significantly overestimated. This shows substantial contamination by older carbon. Hence the radiocarbon ages were rejected. Similar problems with radiocarbon ages were experienced at Lake Burfu located in the carbonate-dominated terrain of the Higher Himalaya where the authors successfully used OSL dating (Beukema et al., 2011).

Environmental magnetic parameters and their temporal variation

A paleoclimatic interpretation of environmental magnetism requires concentration of the magnetic fraction, domain grain type and mineral constituents. The magnetic susceptibility (χlf) indicates the proportional contributions of ferrimagnetic, anti-ferrimagnetic, paramagnetic and diamagnetic concentrations in natural mixtures (soil, sediments). The ferrimagnetic material contains higher values of the χlf and SIRM compared to anti-ferrimagnetic. In contrast, dominance of diamagnetic and paramagnetic minerals (quartz, feldspar, mica) dilutes the values of χlf and SIRM (Verosub and Roberts, 1995; Maiti et al., 2005; Meena et al., 2008, 2011). The magnetic susceptibility of the DG paleolake profile (Fig. 6A) was low at ~12 ka (0.7×10^{-8} m^3 kg^{-1}) and gradually increases to ~11.5 ka (1.2×10^{-8} m^3 kg^{-1}) and then gradually decreases till ~10.2 ka (with fluctuations) to a low value of 0.4×10^{-8} m^3 kg^{-1}. The value shows a sharp increase after 10 ka (1×10^{-8} m^3 kg^{-1}) and then gradually decreases till ~8.5 ka. Following this, a sharp increase in χlf (0.8×10^{-8} m^3 kg^{-1}) continues till ~7 ka. The SIRM follows the trend of χlf and ranges between 15 and 90×10^{-5} Am^2 kg^{-1}, except between ~10.5 and 9.5 ka when it shows an opposite trend with χlf (Fig. 6B).

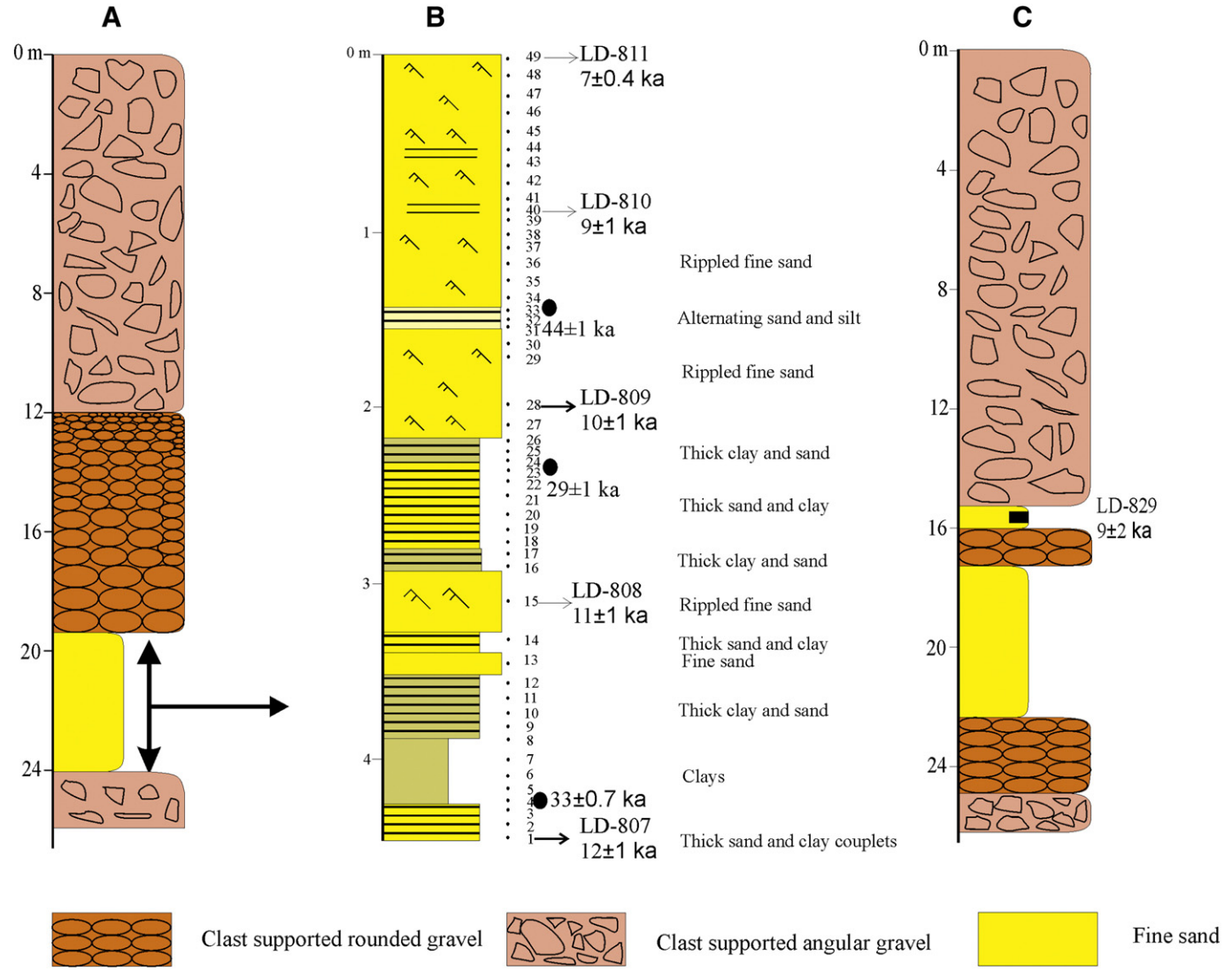

Figure 4. (A) Litholog of section 1. (B) Expanded litholog and Optically Stimulated Luminescence (OSL) chronology (arrows) and ^{14}C dates on extracted organic matter (filled circles) for the lacustrine unit. Note the overestimation and stratigraphic discontinuity in ^{14}C dates. (C) Litholog of section 2 and OSL chronology.

https://doi.org/10.1016/j.yqres.2013.07.006 Published online by Cambridge University Press

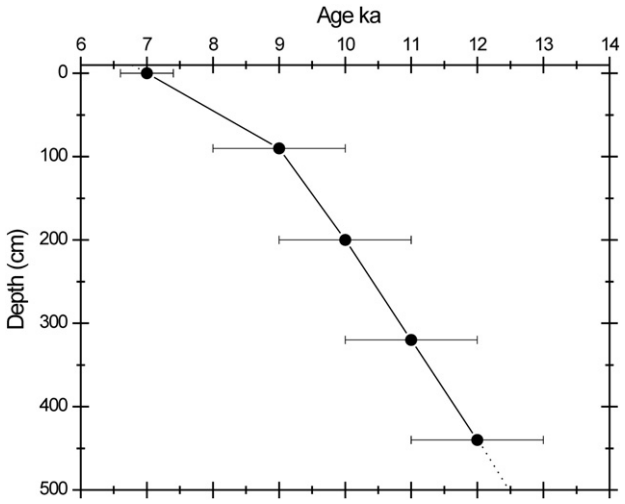

Figure 5. Plot of luminescence ages vs. depth for the studied section. Note that this age model has been used to interpolate the ages in the section.

The ARM responds to the proportional contribution of the magnetic domain grain types. ARM is high for Stable Single Domain (SSD) grains of physical size of 0.1 to 0.01 μm while Pseudo-Single Domain (PSD) grains of physical particle size 20 μm exhibit moderate values of ARM, and the Multi-Domain grains (MD) >20 μm display the lowest values of ARM. The DG paleolake profile (Fig. 6C) shows low concentration of the SSD grains with lowest value (0.6×10^{-8} m^3 kg^{-1}) at ~12 ka that gradually increases (1.2×10^{-8} m^3 kg^{-1}) to ~11 ka. The ARM gradually decreases from ~11 ka to a low value (0.3×10^{-8} m^3 kg^{-1}) at ~10 ka, and then follows the trend of the χlf.

Magnetic mineralogy of the paleolake profile was investigated using two widely used parameters: the S-ratio and coercivity of remanence ($B_{(0)}$cr). The high value of the S-ratio at 12 ka indicates a contribution of anti-ferrimagnetic minerals (Fig. 6D). On the other hand, the $B_{(0)}$cr trend displays a small shift of higher values at the beginning of the profile and remains constant (55 to 60 mT) to 10.5 ka (Fig. 6E). This range of $B_{(0)}$cr rules out the domination of high coercive minerals (hematite or goethite). These minerals in sufficient concentrations will elevate the values of $B_{(0)}$cr above the ferrimagnetic (magnetite or tita-nomagnetite) range because ferrimagnetic minerals have $B_{(0)}$cr <50 mT. A sudden increase and subsequent drop in both $B_{(0)}$cr and S-ratio from10.5 to 10 ka indicates low temperature oxidation that was terminated by a higher influx of ferrimagnetic concentration. A gradual increase in both $B_{(0)}$cr and S-ratio from ~10 to ~7 ka indicates increasing coercivity of the magnetic minerals possibly due to oxidation.

Table 2
^{14}C Chronology of the samples collected from DG paleolake profile.

Sample no.	Depth (cm)	PRL no.	Age (^{14}C ka BP) carbonate	Age (^{14}C ka BP) organic
Malari-3	144	2146	36 ± 1	41 ± 1
Malari-2	237	2145	29 ± 0.5	29 ± 1
Malari-1	430	2144	48 ± 6	33 ± 0.7

Phosphorus speciation analysis

Apatite-bound phosphorus, organic-bound phosphorus and non-apatite-bound phosphorus results are shown in Table 3. The AIP fraction is greater than the NAIP and OP fractions. As the estimated uncertainty in the case of NAIP is relatively high, we use the trends of OP and AIP for further discussion. The NAIP trend is however shown here only to explain that there appears to be negligible transformation of OP to NAIP in the section, as NAIP does not show any increase with depth and OP remains higher than NAIP in most of the samples and most importantly in the lower parts of the sequence. The trends of AIP and OP show complementary patterns (Fig. 7) enabling us to explain climatic conditions in the catchment of the DG paleolake Malari. The comparisons for the excursions are made with respect to the lowest values of 7.8 and 0.74 μmol/g for AIP (DG 10) and OP (DG 28) fractions, respectively. Higher OP flux (with fluctuations) is observed during <12–10 ka (peak value of 3.4 μmol/g at DG 9), ~10–9.2 ka peak value of 4.6 μmol/g at DG 34 and 35 (with a short phase of decline in between) and 8.3–7.4 ka (peak of 3.2 μmol/g at DG 46) (Fig. 7A). An increase in the AIP fraction occurred ca 12 ka (13 μmol/g for DG 1) and a major positive shift occurred at ~10 ka (21.7 μmol/g; DG 29; Fig. 7B).

Discussion

The early Holocene was an interval of major shifts in SW monsoon intensity marked by repeated occurrences of dry and wet spells in the Indian subcontinent, which were contemporaneous with the dry and humid phases of the North Atlantic (Prell and Van Campo, 1986; Fleitmann et al., 2003; Gupta et al., 2003; R.C. Sharma et al., 2004; S. Sharma et al., 2004). Following the early Holocene Optimum, the dry and humid phases in the SW monsoon brought significant changes in the character and rates of sedimentation in the fluvial and lacustrine systems in the Himalaya (Ray and Srivastava, 2010; Beukema et al., 2011). The time-window 12–7 ka is important because it contains information on the pattern of climatic amelioration often called the early Holocene optimum following the termination of the Younger Dryas cold phase. In the Central Himalaya the variability of precipitation depends on the intensification of the Indian summer or SW monsoon and latitudinal shifts in the Inter-Tropical Convergence Zone (ITCZ). At present the Boreal ITCZ reaches a little south of Malari at ~2.1 ± 0.3 km asl

Table 1
Radioactivity, paleodoses and age data for the DG samples.

Lab no.	Sample no.	Depth (m)	U (PPM)	Th (PPM)	K (%)	Paleodoses (Gy)		Dose rate (Gy/ka)	Age (ka)	
						Mean	Least		Mean	Least
LD-807	DGS-1	4.9	3.1	16.7	2.7	62 ± 10	49 ± 5	4.3 ± 0.3	15 ± 3	**12 ± 1**
LD-808	DGS-2	3.2	3.1	13.4	2.3	57 ± 12	45 ± 1	3.9 ± 0.3	14 ± 3	**11 ± 1**
LD-809	DGS-3	2.0	3.7	12.5	2.5	48 ± 6	41 ± 1	3.9 ± 0.3	12 ± 2	**10 ± 1**
LD-810	DGS-4	0.8	2.1	10	2.8	42 ± 6	33 ± 2	3.7 ± 0.2	11 ± 2	**9 ± 1**
LD-811	DGS-5	0.1	2.7	12.1	2.3	39 ± 10	28 ± 1	3.8 ± 0.2	10 ± 3	**7 ± 0.4**
LD-829	DGS-6	15.9	2.3	13.3	2.5	45 ± 5	36 ± 6	3.9 ± 0.1	11 ± 1	**9 ± 2**

Paleodoses estimated using the Single Aliquot Regeneration (SAR) protocol on 30 Aliquots.
Mean of least 10% paleodoses were used for age calculations.
Water content: 5 ± 2% by weight.
Cosmogenic Gamma contribution: 190 ± 30 μGy/a.

https://doi.org/10.1016/j.yqres.2013.07.006 Published online by Cambridge University Press

(Bookhagen and Burbank, 2006). The lake sequence at Malari is located at ~2900 m asl. Thus the catchment of the Malari paleolake lies in an arid to semiarid low rainfall regime (Fig. 1).

The detailed records of environmental magnetism, OP and sand fraction (percent) from DG paleolake profile are now discussed.

Environmental magnetism

In the Malari paleolake profile the high values of magnetic susceptibility are controlled by an increased concentration of the ferrimagnetic fraction (magnetite), a conclusion supported by the low values of the $B_{(0)}$cr and the S-ratio. The ARM, χlf, and SRIM and mineralogy are synchronous strongly suggesting magnetic enhancement and formation of SSD magnetic grains within the lake basin. This kind of enhancement has been widely noticed in Chinese loess and other parts of the world during wet and warm climatic phases or intensified monsoon (Zhou et al., 1990; Maher and Thompson, 1992; Evans and Heller, 2003) Since the Malari paleolake profile also lies at the northern fringe of the SW monsoon regime, the higher values of χlf and lower values of $B_{(0)}$cr and S-ratio are suggestive of an intensified monsoon. Conversely, the values of χlf and SIRM also decreased due to an absence of magnetic enhancement, which increased the contribution of anti-ferrimagnetic minerals, produced in situ by low-temperature oxidation during a dry climate when the lake surface was exposed (Evans and Heller, 2003).

On the basis of the magnetic parameters, we infer that the Malari paleolake profile began with a cold and dry phase at 12 ka when the SW monsoon was weaker, roughly corresponding to the global cooling event of the Younger Dryas (YD). This cold and dry spell was terminated by an abrupt intensification of the summer monsoon from 10 to 9 ka (Fig. 8A). The intensification of the summer monsoon around 10 ka corresponds with the onset of the Holocene Optimum.

Sediment characteristic

The sedimentological details of the section show that it was a consequence of landslide damming of a channel and subsequent formation of a lake. The lake was later breached and taken over by channel processes (bar aggradation) that again were followed by landslide activity. In the Himalaya numerous such paleolake sections can be identified in the higher semiarid monsoon dominated zones where glacial advances (cold phases) would be represented by low sediment flux due to reduced melt water discharge during a weak SW monsoon, whereas coarser sedimentation will represent deglaciation (warmer conditions) during intense SW monsoons (Ariztegui et al., 1997; Juyal et al., 2004). The chronology indicates that the landslide took place at ~12 ka and the landslide dammed lake persisted from 12 to 7 ka. There is ample evidence from the Himalaya that in response to a strengthened monsoon, mass wasting activity, channel damming and formation of lakes increased during the early Holocene (Bookhagen et al., 2005; Sundriyal et al., 2007; Phartiyal et al., 2009). Detailed sand–silt–clay fraction analysis of the lacustrine sequence shows that shortly after ~12 ka, sand contributions to lake increased and there are at least two major sand-rich periods suggesting warmer phases at <12–10.5 ka and 10–9 ka (Fig. 8B). Further, sand percentage in the profile shows no decline from ~8.5 to 7 ka. This is probably due to the shallowing of the lake allowing only coarser sediment to be deposited (Reineck and Singh, 1980).

Phosphorus record

The phosphorus content of a lake unaffected by agricultural fertilizers and sewage depends on two factors: (1) OP produced due to primary productivity of the lake and that supplied from the erosion of soils formed in the catchment, and (2) the AIP supplied in the lake basin from the physical erosion of rocks due to glacial processes or frost and thaw during cold and arid conditions in the catchment. The primary productivity of the DG paleolake must have been negligible as most of the present-day lakes in the Higher Himalaya are oligotrophic (NWIA, 2011). Also under modern conditions, the headwaters of the Dhauliganga River are nutrient-poor (R.C. Sharma et al., 2004). Therefore, the phosphorus in the sediments of this lake profile mainly record input of either the organic productivity of the soil or the apatite inorganic phosphorus due to physical erosion in its catchment.

Following Filippelli and Souch (1999) and Filippelli et al. (2006), the increased OP is believed to indicate increased vegetation cover and soil formation owing to warmer and wetter climate under an intensified SW Indian monsoon. On the contrary, the increase in AIP indicates increased physical weathering of rocks under cold and arid conditions. The phosphorus (both organic and apatite inorganic) trends show significant changes in the supply of AIP and OP to the sediments of the

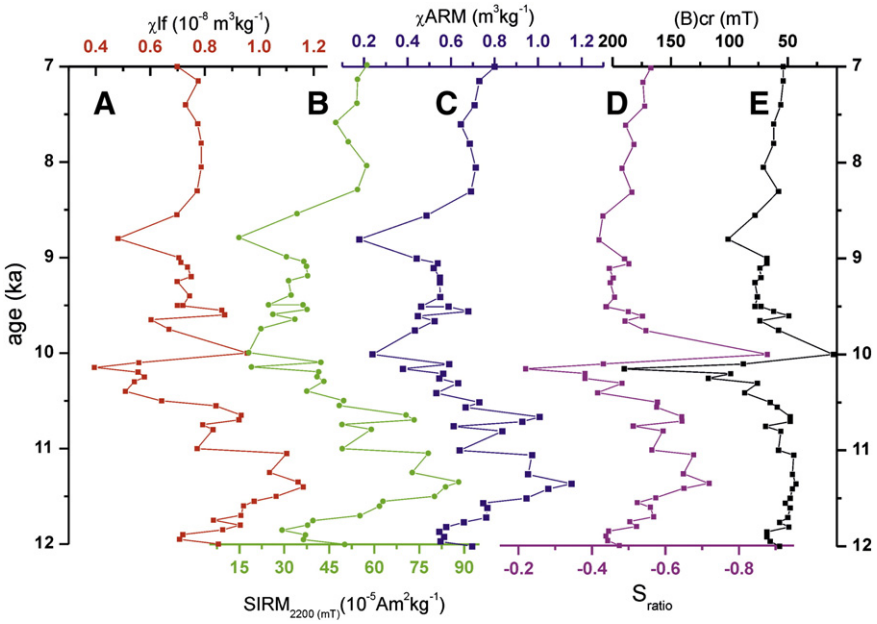

Figure 6. Environmental magnetic parameters (A) magnetic susceptibility (χlf), (B) saturation isothermal remnant magnetization (SIRM), (C) anhysteretic remnant magnetization (ARM), (D) S-ratio, and (E) coercivity of remanance ($B_{(0)}$cr) variation with depth and interpolated ages.

https://doi.org/10.1016/j.yqres.2013.07.006 Published online by Cambridge University Press

Table 3
Phosphorus fractions: organic-bound phosphorus (OP), apatite-bound inorganic phosphorus (AIP), and non-apatite inorganic phosphorus (NAIP) (in μmoles/g) of the DG paleolake profile.

Sample	Depth (cm)	OP μmoles/g	AIP μmoles/g	NAIP μmoles/g
DG 49	0	2.13	9.14	1.04
DG 48	9	1.78	9.49	2.98
DG 47	20	1.97	10.01	1.67
DG 46	29	3.23	9.33	2.49
DG 45	39	2.52	10.94	2.44
DG 44	49	2.20	11.88	1.04
DG 43	60	1.29	11.04	2.40
DG 42	70	1.23	10.98	1.72
DG 41	80	1.10	14.11	2.40
DG 40	90	1.94	11.07	1.72
DG 39	93	1.90	10.85	1.54
DG 38	102	2.55	11.69	2.49
DG 37	110	2.03	9.62	3.07
DG 36	119	4.68	12.82	4.47
DG 35	130	4.58	10.23	4.97
DG 34	140	4.55	10.04	5.65
DG 33	146	3.58	12.75	4.38
DG 32	150	1.65	13.40	0.05
DG 31	155	1.26	15.66	0.45
DG 30	163	3.39	13.59	4.20
DG 29	172	3.49	14.11	4.38
DG 28	200	0.74	21.70	0.72
DG 27	210	3.52	12.04	4.57
DG 26	220	2.91	11.33	5.02
DG 25	227	2.52	10.56	0.77
DG 24	231	2.71	9.39	0.95
DG 23	237	3.68	12.14	4.88
DG 22	247	2.16	11.01	0.63
DG 21	257	2.26	11.24	1.13
DG 20	266	2.68	10.72	1.08
DG 19	276	4.00	10.59	1.76
DG 18	283	2.87	9.27	0.95
DG 17	288	3.13	10.36	1.18
DG 16	298	2.23	10.07	0.50
DG 15	320	2.45	11.65	0.99
DG 14	338	2.71	10.17	1.08
DG 13	350	3.71	9.59	0.95
DG 12	360	1.94	9.49	2.53
DG 11	368	2.87	9.98	2.17
DG 10	376	2.74	7.78	0.99
DG 9	383	3.39	8.56	0.90
DG 8	390	3.26	9.62	0.90
DG 7	400	3.16	8.94	2.21
DG 6	407	2.65	9.49	2.08
DG 5	414	2.81	8.14	2.26
DG 4	421	2.81	8.01	2.80
DG 3	425	2.16	10.98	2.26
DG 2	433	2.03	9.94	1.94
DG 1	440	1.84	12.98	1.99

lake sequence (Fig. 7). Figure 7 clearly shows that increasing OP is complemented by lowering of AIP. Thus percent increase in OP can be considered a warming phase (Fig. 8C). At ~12 ka the lower OP trend suggests that the catchment of the DG paleolake was under cold and arid glacial conditions when physical weathering of the rocks dominated. The scenario changed subsequently when the supply of OP-rich sediments increased at ~10 ka (with intermittent intervals of dry climate). This change indicates development of soil on the slopes of the catchment of the lake and supply of OP to the lake during the deglacial period (Filippelli and Souch, 1999). The dry interval at ~11 ka seems to indicate an erosional phase which cannot be adequately resolved by the OSL dates. Subsequently during the period <11–10.5 ka, the higher OP supply points to soil development under a warm/humid condition (Fig. 8C). The conditions during 10.5 to 10 ka appear to be similar to the previous regime. A pronounced decrease in OP percent at ~10 ka suggests cold and arid conditions (Fig. 8C). During 10–9.0 ka, a pronounced increase in OP supply to the lake suggests a humid spell favoring soil development. During 9–8.4 ka the supply of sediments was mainly through physical erosion indicating a dry spell. However, during 8.3 to 7.4 ka there was some soil development indicating a return of humid condition (Fig. 8C).

The OSL ages have an ~10% uncertainty, equivalent to ~500–1000 years of absolute age. This limits pinpointing a particular climatic event; however, the pattern of early Holocene climatic changes recorded by the sediment proxies is still recognizable using the OSL age model. Despite this limitation all three proxies have captured globally recognized early Holocene (<12–9 ka) climate warming and intensification of the monsoon. Mutual correlations among the proxies are not, at times, statistically significant due to different response times of each proxy to climatic forcing. For instance, organic P is a biological proxy that responds to regional vegetation cover whereas magnetic susceptibility is mainly controlled by the inventory of magnetic minerals.

Early Holocene records of the Summer Monsoon from other regions

It is important to know if the Malari record emulates monsoon rainfall proxy from the: (i) Tso kar humidity record as a proxy of temperature (Wünnemann et al., 2010), (ii) cave records of Oman, (iii) sedimentary sequences of Ganga Plains, and (iv) marine sediments of the Arabian Sea. Also proxy data of the East Asian monsoon should be comparable as recently, based on stable isotope signatures from a stalagmite recovered from Timta cave, Pithoragarh, NW Himalaya. Sinha et al. (2005) suggested that the Indian summer monsoon and East Asian Monsoon strengthened simultaneously.

Tso Kar Lake lies in the NW Himalaya, beyond the northern extremity of the Indian summer monsoon and present study area. This lake record was recently studied to reconstruct the fluctuations in climatic indicators like humidity, surface runoff and vegetation (Wünnemann et al., 2010). The record shows that, in response to warming, there was a continuous rise in lake levels from 12.5 to 10.8 cal ka BP. Furthermore, at ~9.6 cal ka BP and between 8.5 and 7.0 cal ka BP a major rise in water levels took place in response to increased glacial melt. Indian summer monsoon records are also well documented across the Indian subcontinent in cave deposits, marine sedimentary archives in the Arabian Sea, lake records, loess deposits from the Himalaya and fluvial archives of the Ganga Plain. Qunf cave, southern Oman that also lies on the northern limit of the summer migration of the ITCZ and receives ~90% rainfall during the summer months and is at a comparable latitude to the Malari paleolake. The high rainfall phases during 10.5–9 ka to 8–7 ka in the Malari paleolake profile are comparable with a wet phase observed in the Qunf cave during 10.3–8 ka BP (Fig. 8E of this study; Fleitmann et al., 2003). Similarly, Dongge cave records from China that document variations in the East Asian Monsoon suggest an intense monsoon after 12 ka BP with a peak during 9–8 ka BP (Dykoski et al., 2005; Wang et al., 2005). The early Holocene climate amelioration has also been recorded in Sanbao cave, southern China (Dong et al., 2010).

Holocene records in and around the Arabian Sea suggest strong summer monsoon winds and higher rainfall in the early Holocene (Overpeck et al., 1996; Schulz et al., 1998; Neff et al., 2001; Gupta et al., 2003). An Early Holocene increase in continental wetness has also been reported from lake records across the Sahel region of Africa (van Campo et al., 1982; Prell and Van Campo, 1986; Ritchie and Haynes, 1987; Van Campo, 1986; Gasse et al., 1990; Roberts et al., 1993; Lamb et al., 1995; deMenocal, 2000; Gasse, 2000). In the Ganga plain of northern India a wet phase is recognized between 10.8 and 5 cal ka BP (S. Sharma et al., 2004). Soil magnetism/rainfall climo-function analysis from Duowa, western Chinese Loess Plateau, indicates strengthening of the monsoon from 12 to 10 cal ka BP and 8 to 6 cal ka BP (Maher and Hu, 2006).

Thus the paleoclimatic proxy records of the DG lake profile captures early Holocene warming and shows a fair parallelism with the Tso Kar lake record and other regional continental and marine monsoon archives.

https://doi.org/10.1016/j.yqres.2013.07.006 Published online by Cambridge University Press

Malari Paleolake proxy record and climate forcings

General circulation model simulations using the climate parameters of northern summer solar insolation and sea-surface temperature show that, during interglacial conditions, monsoon precipitation is closely related to solar radiation variations. Increasing insolation produces a stronger monsoon (Prell and Kutzbach, 1987). Along with the changes in solar insolation (net solar energy reaching the earth due to variations in orbital parameters) intrinsic solar variability (changes in total solar irradiance; TSI) also played an important role in governing the climate of the last 11,500 cal yr (Mayewski et al., 2004). The Lake Malari record shows strengthened monsoon conditions soon after 12 ka which corresponds to the insolation maxima of ~11 ka (Berger and Loutre, 1991). Concurrence of maxima of χlf at ~11–11.3 ka with contemporaneous summer solar insolation possibly indicates that enhanced summer insolation enhanced the land–sea thermal contrast, thereby intensifying the summer monsoon circulation leading to enhanced precipitation, which probably triggered the landslide and subsequent formation of the studied lake. Thereafter, however, χlf values of the Malari sequence sharply decreased with abrupt changes at ~10.0, 9.5 and 8.8 ka, before stabilizing from ~8.5 ka onwards.

It is tempting to see whether these apparent correlations between the Malari record and solar variability are real. We examined the role of external forcing factors on regional monsoonal conditions by comparing the χlf in lake Malari with contemporaneous millennial-scale variability in summer (June) solar insolation at 30°N (Berger and Loutre, 1991), and a detrended atmospheric ^{14}C record (residual ^{14}C) (Stuiver et al., 1998) in Figure 9. It is apparent that χlf values were at a maximum between ~11 and 11.3 ka (Fig. 9A, green curve), indicating intense summer monsoonal conditions when summer insolation in the

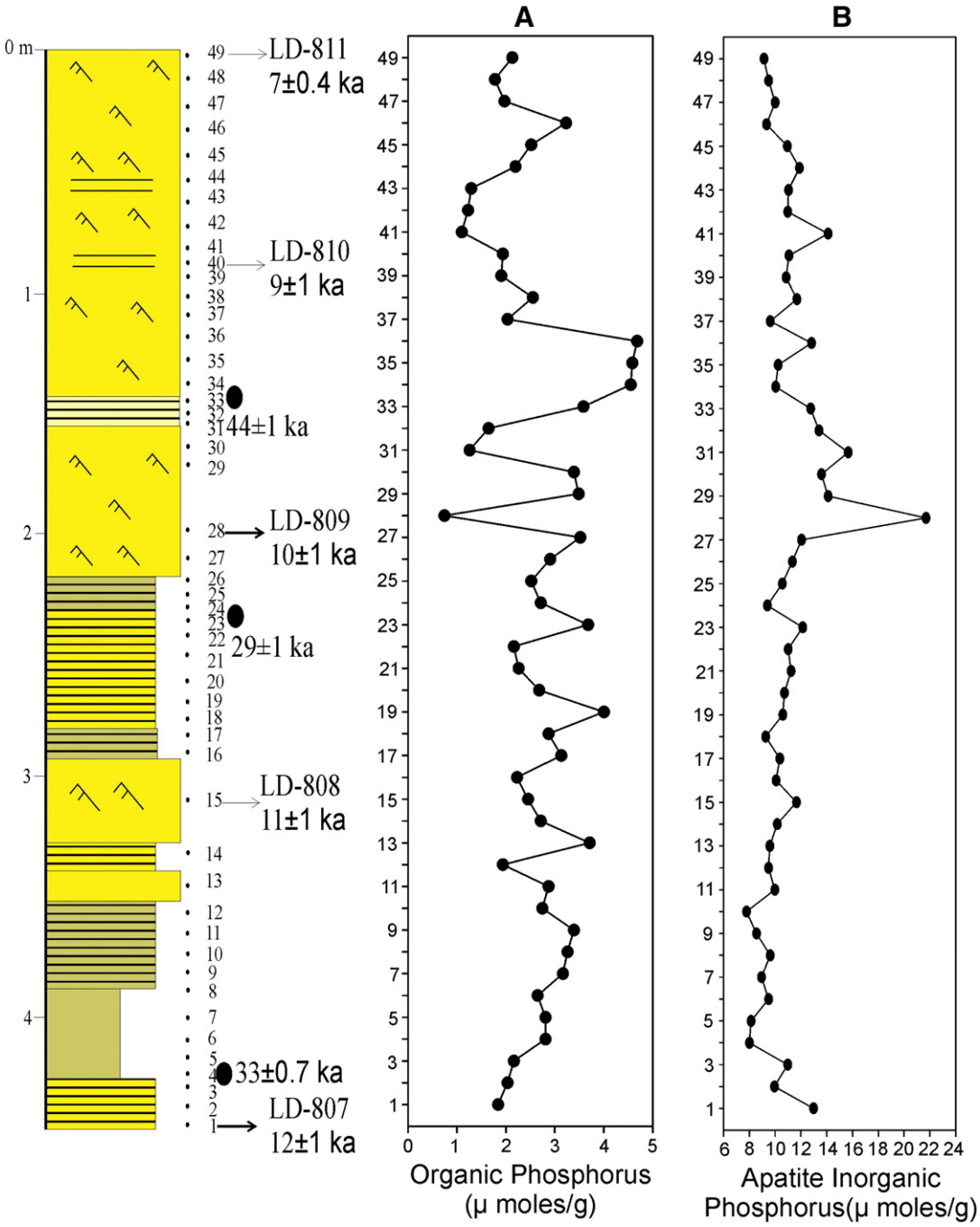

Figure 7. (A) Trends of organic phosphorus (OP) and (B) apatite inorganic phosphorus (AIP) with depths and ages.

https://doi.org/10.1016/j.yqres.2013.07.006 Published online by Cambridge University Press

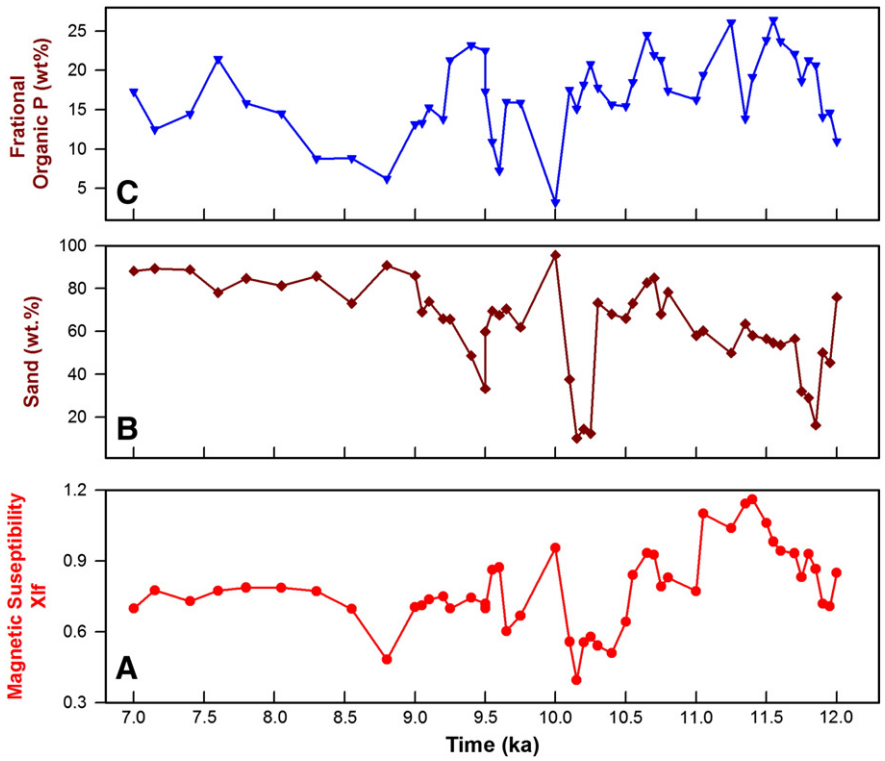

Figure 8. Composite diagram showing the mutual relationships among various parameters (A) magnetic susceptibility, (B) sand percentage, and (C) organic phosphorus. Note that all three show enhanced monsoon conditions during the early Holocene.

northern hemisphere was at a maximum, a period which should be of maximum warmth and hence intense monsoonal activity. Thereafter, however, χlf values sharply decreased with abrupt changes at ~10.0, 9.5 and 8.8 ka, before stabilizing from ~8.5 ka onwards. These fluctuations may have occurred largely due to local reasons. In the Himalaya–Tibet region, it has been shown that the response to climate is complex where, besides solar forcing, the extent of snow cover additionally influences the thermal structure of the atmosphere that in turn

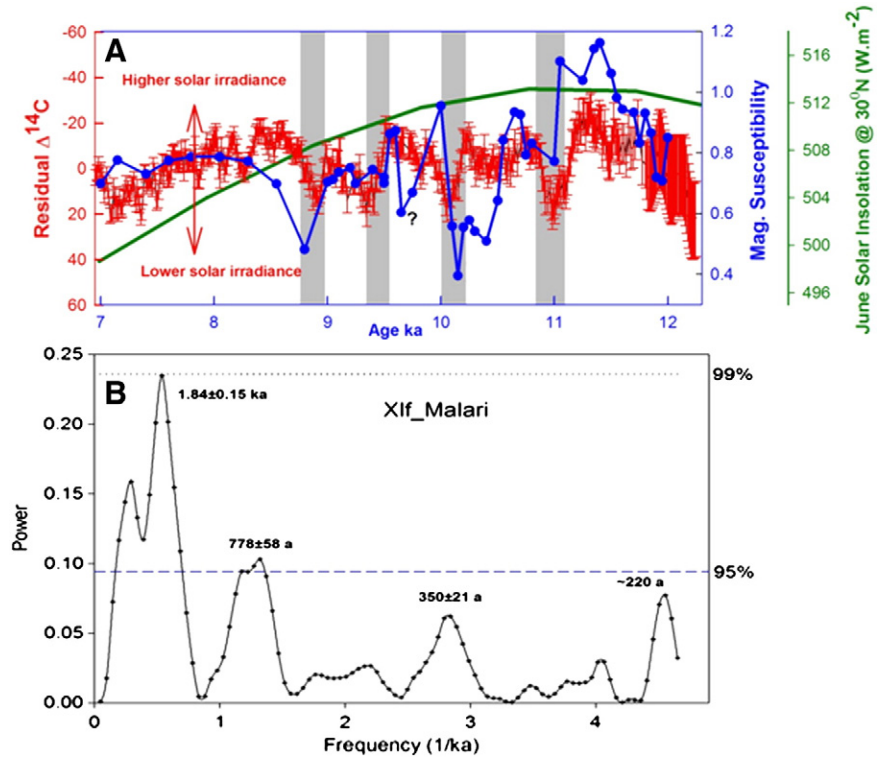

Figure 9. Depth-profile of magnetic susceptibility compared with plausible forcing factors (A) summer solar insolation at 30°N and residual atmospheric $\Delta^{14}C$ variations (see text for discussion). (B) Spectral analysis of magnetic susceptibility data.

https://doi.org/10.1016/j.yqres.2013.07.006 Published online by Cambridge University Press

may control climate variability and rainfall (Staubwasser and Weiss, 2006).

Nonetheless, in order to answer the question: were the observed abrupt/sharp changes in the χlf values of Lake Malari (indicating monsoonal fluctuations) influenced (or triggered) by external solar intrinsic forcing (solar irradiance changes)? We compared the χlf profile with a residual $\delta^{14}C$ record (Fig. 9A; red curve). Though poor temporal resolution of the proxy record at Malari and inherent uncertainties with the age model prevent a detailed cross-correlative statistical analysis, visual inspection of Figure 9A indicates that monsoonal activity in the region changed in tandem with external solar irradiance forcing. Several paleo-monsoonal records of South and Southeast Asia (Neff et al., 2001; Agnihotri et al., 2002; Gupta et al., 2005; Wang et al., 2005; Sinha et al., 2007) have found such an association during the Holocene. It is important to note that the residual $\delta^{14}C$ record is plotted on an inverted scale with lower values of the anomaly indicating higher solar irradiance and vice-versa (Neff et al., 2001; Wang et al., 2005). Close inspection of Figure 9A reveals that sharp declines in external solar forcing (solar irradiance changes) at ~11, 10, 9.5 and 8.9 ka were accompanied by sharply decreasing monsoonal activity as inferred from lower χlf values (as shown by gray bars). Both solar irradiance forcing and χlf values appear to have stabilized after ~8 ka. Despite the lack of correlation analysis for the reasons given earlier, spectral analysis of the χlf depth profile was perfumed using SPECTRUM, a program designed for the inspection of periodicity in unevenly spaced paleo-climatic proxy data (Schulz and Stattegger, 1997). Based on number 49 data points for a time span of 5000 yr, we can only expect dominant cycles in the time domain of 200–2500 yr. Spectral analysis of χlf data as shown in Figure 9C indicates cycles at ~220 yr, 350 ± 21 yr, 778 ± 58 yr and 1840 ± 15 yr that are close to known periodicities of 208 and 232 yr, 385 yr, 805 yr, and 2.24 yr in the residual $\delta^{14}C$ record (Damon and Sonnett, 1991).

Hence, we submit that the lake Malari proxy record of environmental magnetism (χlf) appears to track sharp regional monsoonal changes in the early Holocene, following the 11 ka solar insolation maximum. Better chronologically constrained and temporally resolved paleo-records from this region are likely to reveal further lead/lags between climatic changes and external climate forcing factors.

Conclusions

The following conclusions can be drawn from this study:

1. A landslide-dammed lake in the Garhwal Himalaya was formed at ~12 ka and lasted for ~5 ka. This landslide event corresponds to other such events in the Himalaya.
2. The concentrations of organic-bound phosphorus and apatite-bound inorganic phosphorus as measured through the sediment profile in the lake have a trend that largely follows variations in the Indian summer monsoon between ~12 and ~7 ka. Magnetic susceptibility parameters also corroborate this interpretation.
3. The data suggest that the Garhwal Himalaya received high precipitation in the early Holocene coinciding with the Climatic Optimum when the Indian summer monsoon was intense as observed in cave records from China and Oman and marine records from the Arabian Sea and this climate variability might have been controlled by changes in solar irradiance.
4. This study sets an example for comparison between continental records of precipitation from the Indian landmass and marine records of summer monsoon wind intensity from the Arabian Sea.

Acknowledgment

The Director of WIHG is acknowledged for providing the facilities. PS and YPS acknowledge the Department of Science and Technology for the financial assistance in the form of a research grant# SR/S4/ES-139/2005. M.G. Yadav, Physical Research Laboratory, Ahmedabad is thanked for the ^{14}C dates. Sudipta Sarkar and M. Prakasam helped in plotting the data. AM and JKT thank the Head of the School of Environmental Sciences, JNU, New Delhi for the support. RA acknowledges the Director of NPL for the support. The review provided by Prof. Bob Wasson helped in shaping the text of the manuscript.

References

Agnihotri, R., Dutta, K., Bhushan, R., Somayajulu, B.L.K., 2002. Evidence for solar forcing on the Indian monsoon during the last millennium. Earth and Planetary Science Letters 198, 521–527.
Aitken, M.J., 1998. An Introduction to Optical Dating. Academic Press, London.
Ariztegui, D., Bianchi, M.M., Masaferro, J., Lafargue, E., Niessen, F., 1997. Interhemispheric synchrony of Lateglacial climatic instability as recorded in proglacial Lake Mascardi, Argentina. Journal of Quaternary Science 12, 333–338.
Bagati, T.N., Mazari, R.K., Rajagopalan, G., 1996. Palaeotectonic implications of Lamayuru lake (Ladakh). Current Science 71, 479–482.
Berger, A., Loutre, M.F., 1991. Insolation values for the climate of the last 10 million years. Quaternary Sciences Reviews 10, 297–317.
Beukema, S.P., Krishnamurthy, R.V., Juyal, N., Basavaiah, N., Singhvi, A.K., 2011. Monsoon variability and chemical weathering during the late Pleistocene in the Goriganga basin, higher central Himalaya, India. Quaternary Research 75, 597–604.
Bookhagen, B., Burbank, D.W., 2006. Topography, relief, and TRMM-derived rainfall variations along the Himalaya. Geophysical Research Letters 33, L08405. http://dx.doi.org/10.1029/2006GL026037.
Bookhagen, B., Thiede, R.C., Strecker, M.R., 2005. Late Quaternary intensified monsoon phases control landscape evolution in the northwest Himalaya. Geology 33, 149–152.
Broecker, W.S., 1982. Ocean chemistry during glacial times. Geochimica et Cosmochimica Acta 46, 1689–1705.
Burgisser, H.M., Gansser, A., Pika, J., 1982. Late Glacial lake sediments of the Indus valley area, northwestern Himalaya. Eclogae Geologicae Helvetiae 75, 51–63.
Cronin, V.S., 1989. Structural setting of the Skardu intermontane basin, Karakoram Himalaya, Pakistan. Geological Society of America Special Paper 232, 183–201.
Damon, P.E., Sonnett, C.P., 1991. Solar and terrestrial components of the atmospheric 14C variation spectrum. In: Sonnett, C.P., Giampapa, M.S., Matthews, M.S. (Eds.), The Sun in Time. The University of Arizona Press, Tucson, Ariz, pp. 360–388.
deMenocal, 2000. Abrupt onset and termination of African humid period: rapid climate response to gradual insolation forcing. Quaternary Science Reviews 19, 347–361.
Dong, J., Wang, Y., Cheng, H., Hardt, B., Edwards, R.L., Kong, X., Wu, J., Chen, S., Liu, D., Jiang, X., Zhou, K., 2010. A high-resolution stalagmite record of the Holocene East Asian monsoon from Mt Shennongjia, central China Jinguo. The Holocene 20, 257–264.
Dykoski, C.A., Edwards, R.L., Cheng, H., Yuan, D.X., Cai, Y.J., Zhang, M.L., Lin, Y., Qing, J., An, Z., Revenaugh, J., 2005. A high-resolution, absolute-dated Holocene and deglacial Asian monsoon records from Dongge cave, China. Earth and Planetary Science Letters 233, 71–86.
Evans, M.E., Heller, F., 2003. Environmental Magnetism: Principal and Applications of Environmental magnetism. Academic Press.
Filippelli, G.M., 2002. The global phosphorus cycle. Reviews in Mineralogy and Geochemistry 48, 392–425.
Filippelli, G.M., Souch, C., 1999. Effects of climate and landscape development on the terrestrial phosphorus cycle. Geology 27, 171–174.
Filippelli, G.M., Souch, C., Menounos, B., Atwater, S.S., Jull, A.J.T., Slaymaker, O., 2006. Alpine lake sediment records of the impact of glaciation and climate change on the biogeochemical cycling of soil nutrients. Quaternary Research 66, 158–166.
Fleitmann, D., Burns, S.J., Mudelsee, M., Neff, U., Kramers, J., Mangini, A., Matter, A., 2003. Holocene forcing of the Indian monsoon recorded on a stalagmite from southern Oman. Science 300, 1737–1739.
Fort, M., Burbank, D.W., Freytet, P., 1989. Lacustrine sedimentation in a semiarid alpine setting: an example from Ladakh, northwestern Himalaya. Quaternary Research 31, 332–352.
Galbraith, R.F., Roberts, R.G., Laslett, G.M., Yoshida, H., Olley, J.M., 1999. Optical dating of single and multiple grains of quartz from Jinmium rock shelter, Northern Australia: part I, experimental design and statistical models. Archaeometry 41, 338–364.
Gasse, F., 2000. Hydrological changes in the African tropics since the Last Glacial Maximum. Quaternary Science Reviews 19, 189–211.
Gasse, F., Thehet, R., Durand, A., Gibert, E., Fonte, J.-C., 1990. The arid–humid transition in the Sahara and the Sahel during the last deglaciation. Nature 346, 141–146.
Gupta, A.K., Anderson, D.M., Overpeck, J.T., 2003. Abrupt changes in the Asian southwest monsoon during the Holocene and their links to the North Atlantic Ocean. Nature 421, 354–357.
Gupta, A.K., Das, M., Anderson, D.M., 2005. Solar influence on the Indian summer monsoon during the Holocene. Geophysical Research Letters 32, L17703.
Jain, M., Singhvi, A.K., 2001. Limits to depletion of blue-green light stimulated luminescence in feldspars: implications for quartz dating. Radiation Measurements 33, 883–892.
Juyal, N., Pant, R.K., Basavaiah, N., Yadava, M.G., Saini, N.K., Singhvi, A.K., 2004. Climate and Seismicity in the Higher Central Himalaya during the last 20 kyr: evidences from Garbyang basin, Uttaranchal, India. Palaeogeography, Palaeoclimatology, Palaeoecology 213, 315–330.
Juyal, N., Pant, R.K., Basavaiah, N., Bhushan, R., Jain, M., Saini, N.K., Yadava, M.G., Singhvi, A.K., 2009. Reconstruction of Last Glacial to early Holocene monsoon variability

https://doi.org/10.1016/j.yqres.2013.07.006 Published online by Cambridge University Press

from relict lake sediments of the higher central Himalaya, Uttrakhand, India. Journal of Asian Earth Sciences 34, 437–449.
Kirby, M.E., Lund, S.P., Anderson, M.A., Bird, B.W., 2007. Insolation forcing of Holocene climate change in Southern California: a sediment study from Lake Elsinore. Journal of Paleolimnology 38, 395–417.
Kotlia, B.S., Bhalla, M.S., Shah, N., Rajagopalan, G., 1997a. Palaeomagnetic results from the Pleistocene–Holocene lake deposits of Bhimtal and Bhowali (Kumaun Himalaya) and Lamayuru (Ladakh Himalaya) with reference to the reversal events. Journal of Geological Society of India 51, 7–20.
Kotlia, B.S., Shukla, U.K., Bhalla, M.S., Mathur, P.D., Pant, C.C., 1997b. Quaternary fluviolacustrine deposits of Lamayuru basin, Ladakh Himalaya: preliminary palaeolake investigations. Geological Magazine 134, 807–812.
Lamb, H.F., Gasse, F., Benkaddour, A., EL Hamoutt, N., VanDerKaars, S., Perkins, W.T., Pearce, N.J., Roberts, C.N., 1995. Relation between century-scale Holocene arid intervals in tropical and temperate zones. Nature 373, 134–137.
Maher, B.A., Hu, M., 2006. A high-resolution record of Holocene rainfall variations from the western Chinese Loess Plateau: antiphase behaviour of the African/Indian and East Asian summer monsoons. The Holocene 16, 309–319.
Maher, B.A., Thompson, R., 1992. Paleoclimate significance of the mineral magnetic record of the Chinese loess and paleosols. Quaternary Research 37, 155–170.
Maiti, S., Meena, N.K., Sangode, S.J., Chakrapani, G.J., 2005. Magnetic susceptibility studies of soils in Delhi. Journal of Geological Society of India 66, 667–672.
Mayewski, P.A., Rohling, E.E., Stager, J.C., Karlén, W., Maasch, K.A., Meeker, L.D., Meyerson, E.A., Gasse, F., Kreveld, S. v, Holmgren, K., Lee-Thorp, J., Rosqvist, G., Rack, F., Staubwasser, M., Schneider, R.R., Steig, E.J., 2004. Holocene climate variability. Quaternary Research 62, 243–255.
Meena, N.K., Sangode, S.J., Chakarpani, G.J., 2008. Millennium scale Monsoon variability from Environmental Magnetic record of Sambhar lake, Thar-Desert India. Himalayan Geology 29, 50–51.
Meena, N.K., Maiti, S., Srivastava, A., 2011. Discrimination between anthropogenic (pollution) and lithogenic magnetic fraction in urban soils (Delhi, India) using environmental magnetism. Journal of Applied Geophysics 73, 121–129.
Murray, A.S., Wintle, A.G., 2000. Luminescence dating of quartz using an improved single aliquot regenerative-dose protocol. Radiation Measurement 32, 57–73.
National Wetland Inventory and Assessment, 2011. High Altitude Himalayan Lakes. Space Applications Centre Indian Space Research Organisation, Ahmedabad (21 pp.).
Neff, U., Burns, S.J., Mangini, A., Mudelsee, M., Fleitmann, D., Matter, A., 2001. Strong coherence between solar variability and the monsoon in Oman between 9 and 6 kyr ago. Nature 411, 290–293.
Overpeck, J.T., Anderson, D.M., Trumbore, S., Prell, W.L., 1996. The southwest monsoon over the last 18,000 years. Climate Dynamics 12, 213–225.
Phartiyal, B., Sharma, A., Srivastava, P., Ray, Y., 2009. Chronology of relict lake deposits in the Spiti River, NW Trans Himalaya: implications to Late Pleistocene–Holocene climate–tectonic perturbations. Geomorphology 108, 264–272.
Prell, W.L., Kutzbach, J.E., 1987. Monsoon variability over the past 150,000 years. Journal of Geophysical Research 92, 8411–8425.
Prell, W.L., Van Campo, E., 1986. Coherent response of Arabian Sea upwelling and pollen transport to late Quaternary monsoonal winds. Nature 323, 526–528.
Preusser, F., Chithambo, M.L., Götte, T., Martini, M., Ramseyer, K., Sendezera, E.J., Susino, G.J., Wintle, A.G., 2009. Quartz as a natural luminescence dosimeter. Earth-Science Reviews 97, 184–214.
Ray, Y., Srivastava, P., 2010. Widespread aggradation in the mountainous catchment of the Alaknanda–Ganga River System: timescales and implications to Hinterland–foreland relationships. Quaternary Science Review 29, 2238–2260.
Reineck, H.E., Singh, I.B., 1980. Depositional Sedimentary Environments. Springer Verlag, Heidelberg (549 pp.).
Ritchie, J.C., Haynes, C.V., 1987. Holocene vegetation zonation in the eastern Sahara. Nature 330, 645–647.
Roberts, N., Taieb, M., Barker, P., Damnati, B., Icole, M., Willaimson, D., 1993. Timing of the Younger Dryas event in East Africa from lake-level changes. Nature 366, 146–148.
Ruban, V., Lopez-Sanchez, J.F., Quevauviller, Ph., 2002. Validation of a standards method for evaluating phosphorus forms within sediments. Bulletin Des Laboratories Des Ponts Et Chaussees 240 (4409), 43–52.
Ruttenberg, K.C., 2007. The global phosphorus cycle: overview. The Treatise on Geochemistry, vol. 8. Elsevier ltd., pp. 585–643 (Chapter 8.13).
Schulz, M., Stattegger, K., 1997. SPECTRUM: spectrum analysis of unevenly spaced paleoclimatic time series. Computers and Geosciences 23, 929–945.
Schulz, H., von Rad, U., Erlenkeuser, H., von Rad, U., 1998. Correlation between Arabian Sea and Greenland climate oscillations of the past 110,000 years. Nature 393, 54–57.
Sharma, R.C., Bhanot, G., Singh, D., 2004a. Aquatic macroinvertebrate diversity in Nanda Devi Biosphere Reserve, India. The Environmentalist 24, 211–221.
Sharma, S., Joachimski, M., Sharma, M., Tobschall, H.J., Singh, I.B., Sharma, C., Chauhan, M.S., Morgenroth, G., 2004b. Lateglacial and Holocene environmental changes in Ganga Plain, Northern India. Quaternary Science Reviews 23, 145–159.
Shroder, J.F., Khan, M.S., Lawrence, R.D., Madin, I.P., Higgins, S.M., 1989. Quaternary glacial chronology and neotectonics in the Himalaya of northern Pakistan. Geological Society of America Special Paper 232, 275–294.
Shukla, U.K., Kotlia, B.S., Mathur, P.D., 2002. Sedimentation pattern in a trans-Himalayan Quaternary lake at Lamayuru (Ladakh), India. Sedimentary Geology 148, 404–423.
Sinha, A.K., 1989. Geology of Higher Central Himalaya. John Wiley and Sons (219 pp.).
Sinha, A., Cannariato, K.G., Stott, L.D., Li, H.-C., You, C.-F., Cheng, H., Edwards, R.L., Singh, I.B., 2005. Variability of southwest Indian summer monsoon precipitation during the Bolling-Allerod. Geology 33, 813–816.
Sinha, A., Cannariato, K.G., Stott, L.D., Cheng, H., Edwards, R.L., Yadava, M.G., Ramesh, R., Singh, I.B., 2007. A 900-year (600 to 1500 A.D.) record of the Indian summer monsoon precipitation from the core monsoon zone of India. Geophysical Research Letter 34. http://dx.doi.org/10.1029/2007GL030431.
Slaymaker, O., Souch, C., Menounos, B., Filippelli, G., 2003. Advances in Holocene mountain geomorphology inspired by sediment budget methodology. Geomorphology 55, 305–316.
Srivastava, P., Tripathi, J.K., Islam, R., Jaiswal, M.K., 2008. Fashion and phases of Late Pleistocene aggradation and incision in Alaknanda River, western Himalaya, India. Quaternary Research 70, 68–80.
Srivastava, P., Bhakuni, S.S., Luirei, K., Misra, D.K., 2009. Fluvial records from the Brahmaputra River exit, NE Himalaya: climate–tectonic interplay during Late Pleistocene–Holocene. Journal of Quaternary Science 24, 175–188.
Staubwasser, M., Weiss, H., 2006. Holocene climate and cultural evolution in late prehistoric–early historic West Asia. Quaternary Research 66, 372–387.
Stuiver, M.P.J., Reimer, E., Bard, J.W., Beck, G.S., Burr, K.A., Hughen, B., Kromer, F., McCormac, G., Plicht, J.v. d, Spurk, M., 1998. INTCAL98 radiocarbon age calibration, 24,000–0 cal BP. Radiocarbon 40, 1041–1083.
Sundriyal, Y.P., Tripathi, J.K., Sati, S.P., Rawat, G.S., Srivastava, P., 2007. Landslide-dammed lakes in the Alaknanda Basin, Lesser Himalaya: causes and implications. Current Science 93, 568–574.
Teed, R., Umbanhower, C., Camill, P., 2009. Multiproxy lake sediment records at the northern and southern boundaries of the Aspen Parkland region of Manitoba, Canada. The Holocene 19, 937–948.
Tiessen, H., Stewart, J.W.B., Cole, C.V., 1984. Pathways of transformations in soils of differing pedogenesis. Soil Science Society of America Journal 48, 853–858.
Van Campo, E., 1986. Monsoon fluctuations in two 20,000-yr B.P. oxygen-isotope/pollen records off southwest India. Quaternary Research 26, 376–388.
Van Campo, E., Duplessy, J.C., Rossignol-Strick, M., 1982. Climatic conditions deduced from a 150-kyr oxygen isotope pollen record from the Arabian Sea. Nature 296, 56–59.
Verosub, K.L., Roberts, A.P., 1995. Environmental magnetisim: past, present and future. Journal of Geophysical Research 100, 2175–2192.
Wang, Y., Cheng, H., Edwards, R.L., He, Y., Kong, X., An, Z., Wu, J., Kelly, M.J., Dykoski, C.A., Li, X., 2005. The Holocene Asian monsoon: links to solar changes and North Atlantic climate. Science 308, 854–857.
Williams, J.D.H., Syers, J.K., Shukla, S.S., Harris, R.F., Armstrong, D.E., 1971. Levels of inorganic and total phosphorus in lake sediments as related to other sediment parameters. Environmental Science and Technology 5, 1113–1120.
Wünnemann, B., Demske, D., Tarasov, P., Kotlia, B.S., Reinhardt, C., Bloemendal, J., Diekmann, B., Hartmann, K., Krois, J., Riedel, F., Arya, N., 2010. Hydrological evolution during the last 15 kyr in the Tso Kar lake basin (Ladakh, India), derived from geomorphological, sedimentological and palynological records. Quaternary Science Reviews 29, 1138–1155.
Zhou, L.P., Oldfield, F., Wintle, A.G., Robinson, S.G., Wang, J.T., 1990. Partly pedogenic origin of magnetic variations in Chinese loess. Nature 346, 737–739.

https://doi.org/10.1016/j.yqres.2013.07.006 Published online by Cambridge University Press